Comparison of different techniques for the monitoring of the Lüders bands development

J. Petit[1], D. Wagner[1], N. Ranc[2], G. Montay[3], M. François[3]

[1] LEME, EA4416, Université Paris Ouest, 92410 Ville d'Avray, France
[2] PIMM, CNRS, 151 Bd de l'Hôpital, 75013 Paris, France
[3] LASMIS, UMR CNRS 6279, University of Technology of Troyes, 10010 Troyes, France

In C-Mn and some low alloyed steels, the plastic deformation begins by a macroscopic heterogeneous strain which materializes into the propagation of a strain band along a tensile sample with a uniform cross-section. This band is named Lüders, or Piobert-Lüders, band and it is considered by some authors as a plastic wave. This particular strain localization, which goes through the length of the sample, is explained by an avalanche phenomenon which enables step by step to unfix the dislocations from their Cottrell's atmosphere. However, although its effects are well enough known, one knows much less its causes. In this paper, the travel of the Lüders band is monitored thanks to several techniques based on different physical principles: optical (speckle interferometry), thermal (infrared pyrometry) and acoustic (acoustic emission). The position of the band, its inclination, its propagation speed and the strain rate inside the band are the main points of comparison between each technique. They allow verifying some features about the propagation of the bands and giving some new assumptions about their formation and their development.

Keywords Lüders Band, Strain Localization, Infrared Thermography (IRT), Electronic Speckle Pattern Interferometry (ESPI), Acoustic Emission (AE), Tensile Test

1. Introduction

Plastic strain localization is a major problem in metalworking situations. In ductile metals, macroscopic plastic deformation heterogeneities such as Lüders bands [1-3], Portevin-Le Châtelier effect [4-6] or necking [7-10] can occur. Lüders bands and Portevin-Le Châtelier bands, in particular type A and type B, propagate in some metallic alloys for specific temperatures and strain rate conditions. This last localization phenomenon is described in many papers [11-14]. In ductile metals, the onset of necking is well referenced in literature and is particularly important for the characterization of the forming limit diagram [15-16].

Lüders bands propagation often occurs in hot-rolled low-carbon steels deformed or annealed at 300°C (static ageing). These bands are observed in ferritic phase of steels and form unaesthetic patterns on the material surface. They appear when the plastic deformation starts and disappear early. In uniaxial tensile test, Lüders bands propagate all along the gauge length of the specimen. Indeed, when interaction energy is strong between dislocations and solute atoms which can easily diffuse, like carbon and nitrogen atoms in iron, they gather around dislocations to form Cottrell's atmospheres. Dislocations are strongly anchored and a considerable stress is necessary to release them. Very often, this stress level is reached first in a point of the metal as the result of local effect of stress concentration, notably, in uniaxial tensile test, at the fillet radius with the specimen heads. Deformation remains localized in a narrow zone, corresponding to a Lüders band. The stress concentrations at the band front enable a gradual unlocking of the dislocations in the non-deformed part of the specimen. Thus, this process activates an avalanche that, from grain to grain, goes through all the polycrystal; there is band propagation [17-18]. Besides, the band propagates under a macroscopic stress, R_e^l, lower than the one, R_e^u, needed for initiation.

In order to go further concerning origins and activation modes understanding of this specific deformation mechanism, full-field measurements methods: Infrared Thermography (IRT) [19],

Electronic Speckle Pattern Interferometry (ESPI) and Acoustic Emission (AE) [3] are used, sometimes combined, and compared.

2. General experiments description

Lüders bands were studied during tensile test on two hot-rolled low-carbon steels: one S235 (0.16%wt Carbon) and one C35 (0.35%wt Carbon) according to the European standard. Both are centered cubic (cc) ferritic steels with pearlite. For the first one, propagation of the bands was followed by IRT. For the second one, propagation was followed by AE sole and by ESPI and AE simultaneously. Note that these two experiments were performed in two different laboratories, on two different tensile machines. One knows that the stiffness of the tensile machine can modify the Lüders bands generation and propagation. Here, machines are supposed stiff enough to have an insignificant influence on the Lüders bands behavior. In the future, coupling of the three investigation techniques is foreseen on the same machine.
Dog-bone like specimens with rectangular cross-section are used for the tests. The planar surfaces of the specimens are convenient for 2-D thermal and kinematics full-field measurements techniques and to fix acoustic sensors. The dimensions of the specimens are given on the Fig. 1. Although their influence was not studied here, curvature of the fillet radius are also reported.

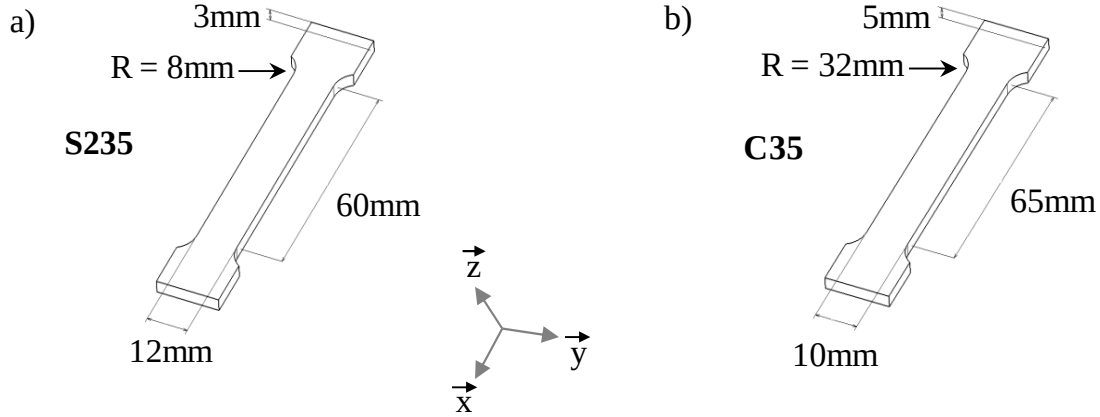

Figure 1. Scheme of the specimens: a) S235 and b) C35.

The initial microstructure of the as received materials is characterised by a grain size ranging between 10 and 15 µm for the S235 and 5 and 10 µm for the C35. The roughness of the S235 specimen is Ra / Rt ≈ 2.0 / 15 µm, the C35's one is Ra / Rt ≈ 5.3 / 35 µm.

3. IRT as Lüders bands following technique

3.1. Experimental procedure

Tests on the S235 steel were performed at 10 mm.min^{-1} on a hydraulic tensile machine with a 100 kN load cell. The stiffness of the machine is 156 kN.mm^{-1}. To characterize temperature increase due to the Lüders bands, specimens were placed in front of an infrared CCD camera. The camera model is a Cedip Silver Orion MW F/3 with InSb detectors. The size of the camera matrix and the spatial resolution are respectively about 320 x 256 pixels and 0.25 mm per pixel. The aperture time is fixed at 1000 µs. The refresh frequency of the camera is of 33 Hz, which corresponds to a duration between two pictures of 30.3 ms. Others acquisition parameters are given in Table 1. Under these conditions, the noise of the camera is about 25 mK. A calibration with a black body allows to deduce the links between the specimen surface temperature and the camera signal. In order to reduce the effect of the emmittance of the material surface, the samples were covered with black paint to get an emissivity close to 1.

Table 1. Acquisition parameters of the IRT device used during tensile test on the S235 steel.

Integration time	Frame rate	Bandwidth	Room temperature
1000 µs	33.33 Hz	3.7 - 4.8 µm	22.5°C

In most of metallic materials, during quasi-static tests at room temperature, plastic deformation goes with thermal energy dissipation, which is the result of dislocations movements inside grains. Another part, less important, of the mechanical energy brought to deform the sample is stored in the material. Thus, the temperature variation is related to the plastic deformation through the following relation [20]:

$$\rho c_p \dot{T} = \beta \underline{\underline{\sigma}} : \underline{\underline{\dot{\varepsilon}_p}} + \lambda \Delta T \quad (1)$$

where ρ is the density, c_p the specific heat, T the temperature, the symbol " $\dot{}$ " for the time derivative, β the Taylor-Quiney coefficient, $\underline{\underline{\sigma}}$ the stress tensor, $\underline{\underline{\dot{\varepsilon}_p}}$ the plastic deformation rate tensor, λ the thermal conductivity and the symbol Δ for the Laplacian.

More particularly, $\rho c_p \dot{T}$ represents the calorific power related to the atomic excitement. $\beta \underline{\underline{\sigma}} : \underline{\underline{\dot{\varepsilon}_p}}$ is the mechanical-thermal coupling term related to the dissipative thermal energy, which represents $100 \times \beta$ % of the energy creation inside the material; the other part corresponding to the stored energy. $\lambda \Delta T$ represents the thermal transfers by conduction.

During the Lüders band propagation and along an increment of plastic deformation, given the weak thermal conductivity of the S235 steel, the term $\lambda \Delta T$ in the Eq. 1 can be ignored such as the band propagation is adiabatic. Eq. 1 becomes:

$$\rho c_p dT = \beta \underline{\underline{\sigma}} : d\underline{\underline{\varepsilon_p}} \quad (2)$$

Consequently, if the constitutive law of the material is known, then the temperature variation is fully representative of the plastic deformation.

3.2. Thermal following of the Lüders band

The beginning of the tensile test (total strain under 10%) of the S235 steel followed by IRT is shown on Fig. 2. All the IRT images recorded during tensile test and shown in Fig. 2 were subtracted with the first image (0% of total strain) to get the temperature variation during the test. A constant scale with boundaries close to the max and the min values met through the 12 images sequence is chosen.

In the beginning of the tensile test, the temperature decreases. The associated homogeneous temperature variation is about -0.40°C until the upper yield stress R_e^u. Just before the upper yield stress (3rd image), a raising of the temperature corresponding to the beginning of the plastic deformation localization can be observed simultaneously near the two specimen edges. When stress is enough, a plastic deformation band, which makes growth the temperature on its way, leaves one side of the specimen to join the other one, deformation localization in the second edge fades; this phenomenon is typical of the Lüders band propagation.

On the 8th image, a second band is forming at the upper end of the specimen. But, this one will be rapidly absorbed by the main band. When the Lüders band stops, plastic deformation tends to become more and more homogeneous along the specimen.

The temperature recordings at the points 1, 2 and 3 (Fig. 2) show a sudden increase in the temperature when the band goes in front of the measurement point. After the band goes beyond each point, it can be remarked that the temperature remains constant, what means that neither elastic nor plastic strains take place; the specimen keeps the heat generated during the band passing.

Moreover, the amplitude of temperature reached after the band passing is observed to increase during the propagation, what means the properties of the Lüders band could change.

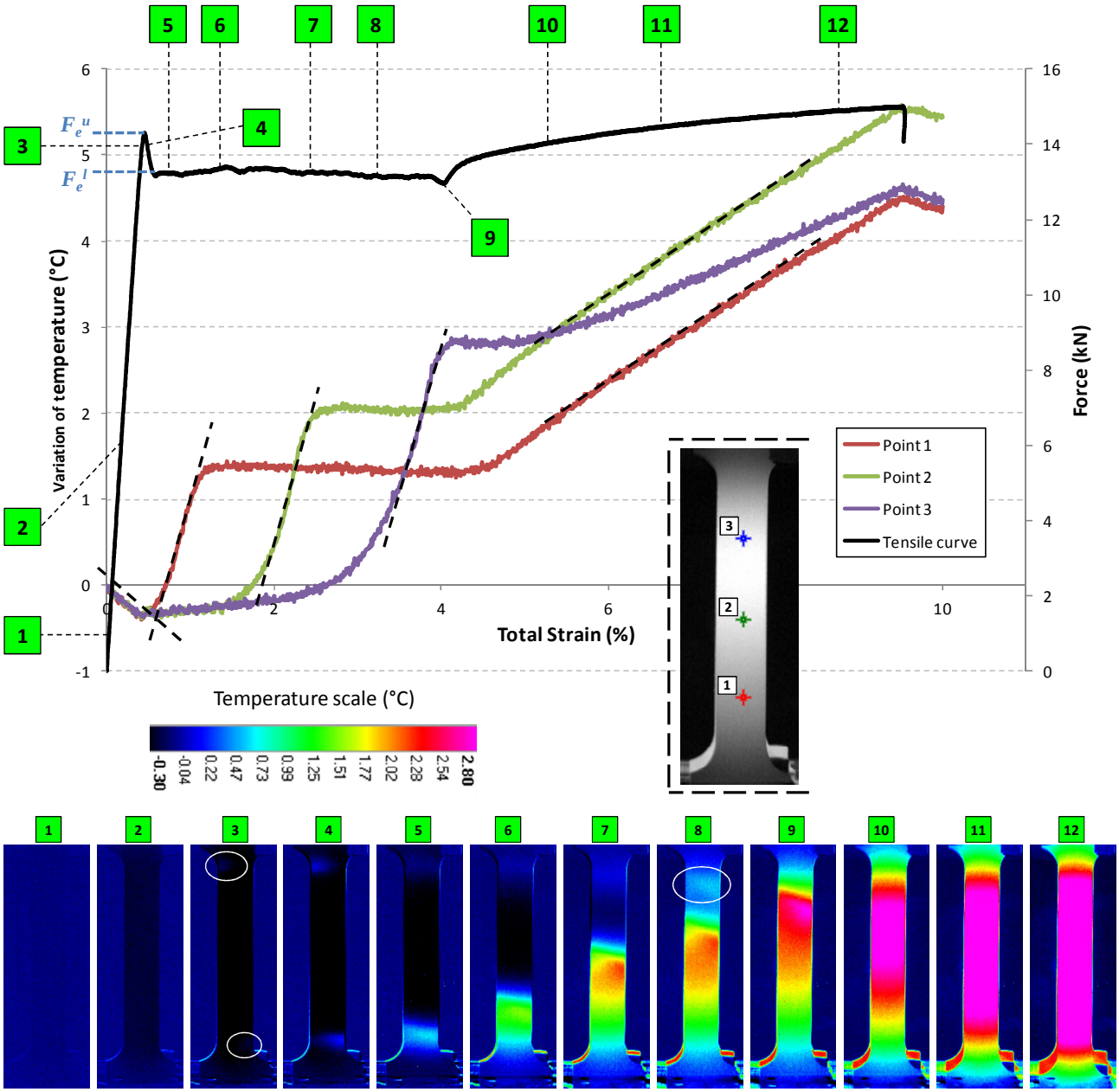

Figure 2. IRT maps obtained while the first 10% of total strain of a S235 steel. The tensile curve (black line) and the temperature evolution (red, green and blue lines) for three points placed on the specimen (see inset) are also depicted. The tensile forces F_e^u and F_e^l corresponding to the upper and lower yield stresses are showed on the tensile curve.

In order to be more sensitive to local variations of temperature on a short period, each image was subtracted with another one which arrives 0.6 s before. Fig. 3(a) shows the new type of obtained image. According to the IRT pictures, the velocity of the band propagation seems constant and approximately 24 times the crossbeam speed v_t. The inclination angle of the band varies hardly during propagation, it is mostly about 60° with respect to the tensile axis. For a given band position, temperature profiles of each line (Fig. 3) show maxima which don't superimpose, what proves the band is tilted.

The shape of the temperature profiles can be fitted by a Lorentz function, like proposed in [21], to deduce the maximum and the integral width of the band. It is found that the maximum is approximately 0.7°C and the integral width 11 mm. Both values strongly depend on the time

elapsed between the two subtracted images. In addition, this value is probably overestimated because of the conduction phenomenon which tends to spread the band.
It is also interesting to note the temperature profile associated to the line 3 on Fig. 3 presents a small negative hook to the rear of the band. This negative hook certainly corresponds to a tensile elastic stress which is higher in this zone than anywhere else. So, is it a consequence of the band propagation or does this tensile state contribute to the successive dislocations unpinning ? In addition, the temperature profile associated to the line 1 presents a small positive hook to the rear of the band. This one could correspond to an elastic compression state. By following this idea and by noticing that the temperature profile associated to the line 2 presents neither a negative nor a positive hook to the rear of the band, it can be assumed that the part of the specimen behind the band rotates.

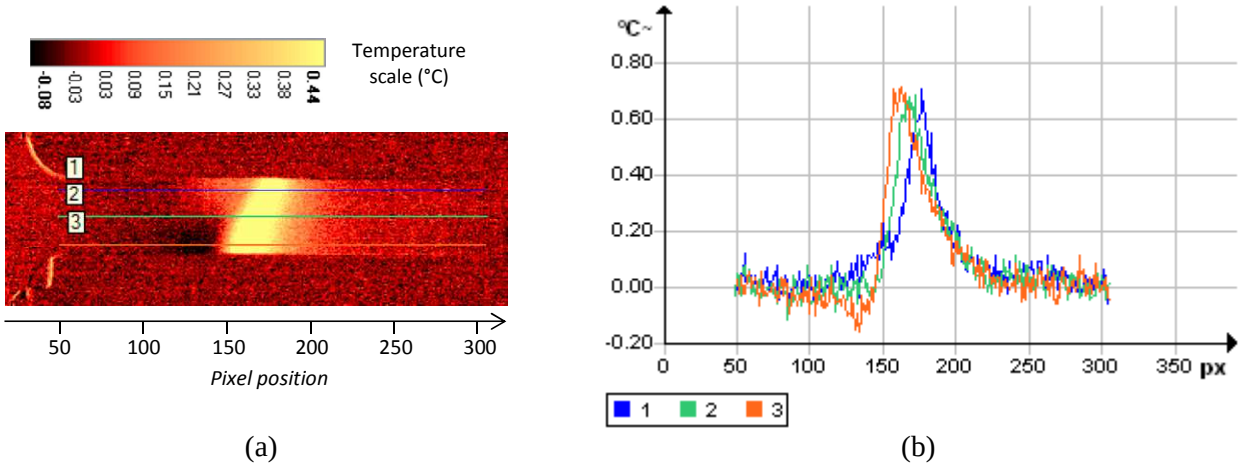

(a) (b)

Figure 3. (a) Typical recomputed image (differences between two original images separated of 0.6 s) obtained during Lüders band propagation in a S235 steel. (b) Temperature profiles along three lines uniformly distributed through the specimen width (see (a)).

Finally, after the Lüders band passing, when the deformation is homogeneous in the specimen (last images on Fig. 2), the temperature is about constant on the whole surface of the gauge length of the specimen and raises much slower than during Lüders band propagation.

4. ESPI and AE as Lüders bands following techniques

4.1. Experimental procedure

Tests on the C35 steel were performed on a 150 kN capacity tensile machine at different crossbeam speeds. The experimental setup, mainly including the speckle interferometer, the acoustic sensors and the tensile machine, is presented on Fig. 4. The theoretical principles of ESPI and AE can be found respectively in reference books [22, 23] and [24]. At the sample scale, ESPI offers a better resolution, one or two orders of magnitude, on material displacements than DIC (Digital Image Correlation) or photoelasticity. Nevertheless, after surface coating preparation, DIC gives direct access to two sensibility vectors without additional equipment [2]. When sample surface is coated with birefringent resin, photoelasticity, as for it, allows to reveal naked-eye Lüders bands [25].
In the present case, the speckle interferometer setup is an in-plane sensitive configuration, known as a Leendertz set-up, with a sensitivity vector $\vec{s}$ parallel to the tensile direction. Speckle patterns are recorded on a CCD camera (1280 pixels × 980 pixels, monochromatic, 8 bits) with a 5µm spatial resolution. One of the mirrors is mounted on a piezo-electric transducer generating optical path differences by translation; it enables to get the phase of the interference pattern at all pixels of the image and obtain a better resolution on measured displacements (~25 nm in practice).

Note that no preparation of the surface of the specimens was performed for ESPI measurements. The surfaces were sufficiently rough to generate the speckle patterns and not too much to keep the plane surface hypothesis and avoid a premature localization.

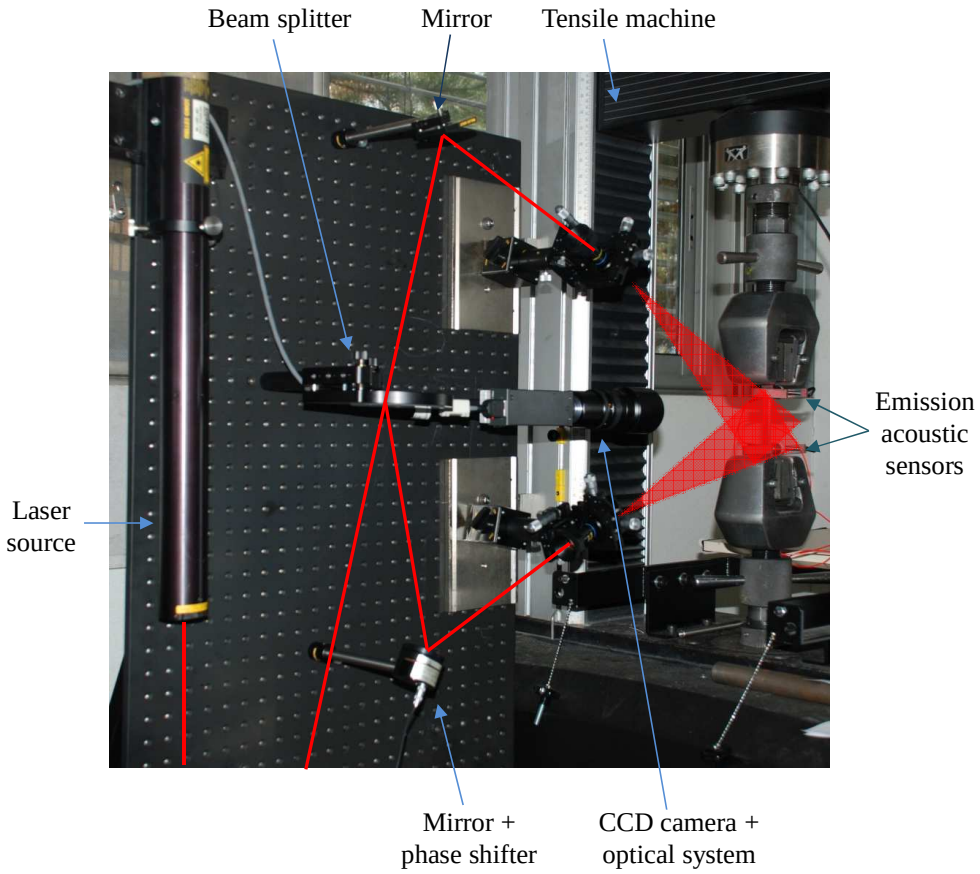

Figure 4. Experimental setup: in-plane speckle interferometer and micro-tensile machine. The laser beam path is schematized as a red line.

For AE measurements, two large-band (50 – 600 kHz) piezo-electric sensors were used. They convert acoustic signal into electric signal machine readable. These sensors are elastically maintained on the surface specimen with the same tension all along the test, Fig. 5. Because of the small size of the specimen heads, sensors are located near the fillet radius. To ensure the crossing of the acoustic wave between the specimen and the sensor, a coupling fluid (thixotropic gel) is inserted between both of them. The electric signal received by each sensor is amplified by a 40 dB pre-amplifier with a 1 MHz cut-off frequency, and then the electric signal is sent towards the acquisition card of the AEwin system (Euro Physical Acoustics). This latter gives intrinsic parameters related to the signals like amplitude, duration, energy, etc...

Many acoustic events do not come from the material been deforming, but they can come from the tensile machine working, slip of the sensors on the sample surface, micro-slips of the sample into the jaws, external noise… So, thanks to an acoustic events localization treatment, it is possible not to take into account those parasite events in the future analysis. The acoustic events localization requires at least two sensors set on the specimen and it enables to know, in our case, the position of the event sources along the gauge length of the specimen with an accuracy of about 5 mm. Given the small size of the specimens, the recorded signal for one acoustic event is a combination of the longitudinal wave, the transversal wave and possibly also some reverberated waves. For localization, longitudinal wave speed is considered, especially since the sensors are more sensible to this type of wave.

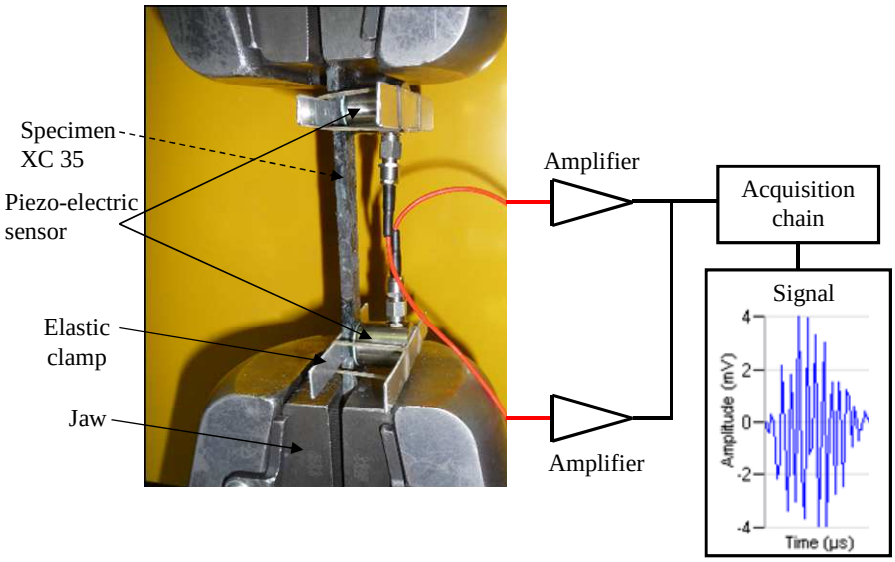

Figure 5. Scheme of the AE setup mounted on tensile specimen.

4.2. AE analysis

The Fig. 6, in a Event Amplitude versus Total Strain representation, shows all the detected events all along a tensile test performed at 0.5 mm.min^{-1}, with a signal amplitude higher than an arbitrary threshold (30 dB). It can be observed that until the disappearance of the Lüders band, a lot of events were detected. About 75% of the total acoustic activity corresponds to only 3% of the total strain, knowing that fracture occurs at 31.1% of the total strain. This observation is consistent with the fact of the band propagation produces a spectacular increase of the mobile dislocations density [26]. In the 5086-0 aluminium alloy [27], Baram also observed that deformation in the Lüders band region generated an high acoustic activity.

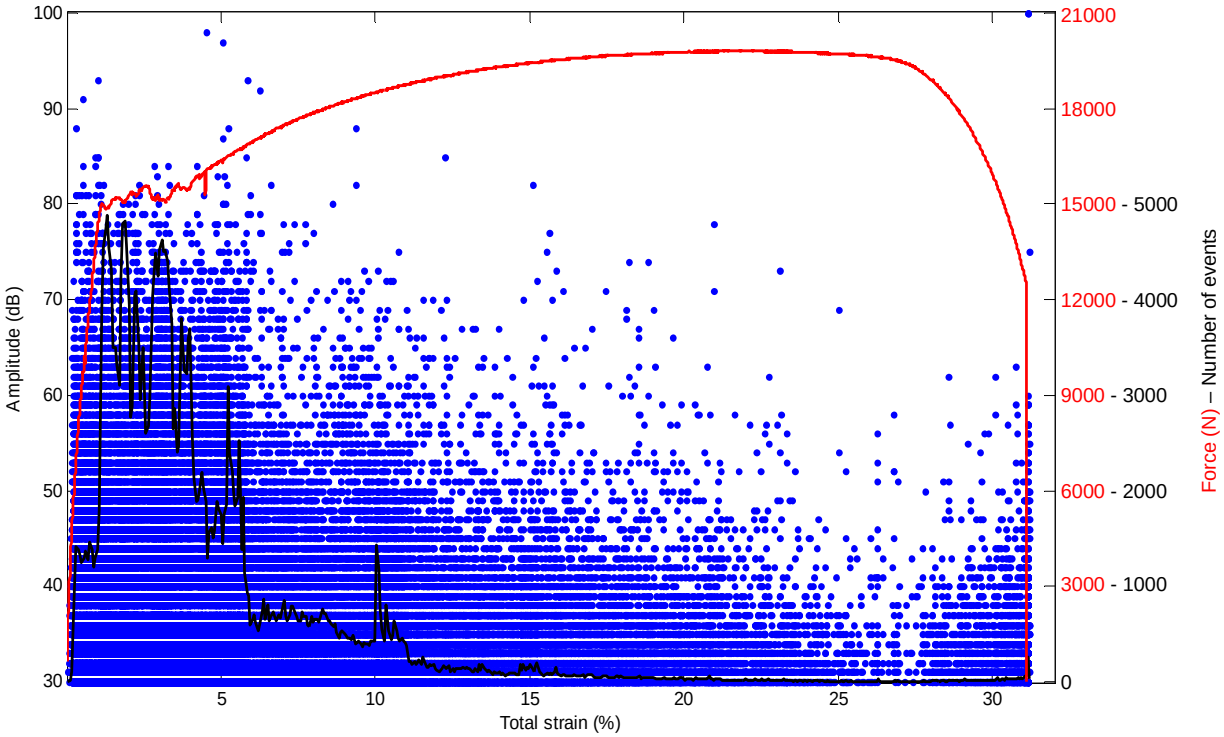

Figure 6. Amplitude versus Total Strain representation of the acoustic events recorded on the two sensors during tensile test of a C35 steel. The tensile curve (red line) and the number of events collected on a 5s time range (black line) are also depicted.

It can be highlighted that the number of events is very variable on a given short duration during the Lüders band propagation. AE activity shows important fluctuations and it can be remarked that this activity presents some intense local maxima when the tensile load presents local minima. Conversely, the AE activity presents some local minima when the tensile load presents maxima. Consequently, that means an important dislocation activity appears for each loading drop, as if each maximal local stress could unpin a lot of dislocations anchored in a certain neighborhood. This unpinning making fall down the stress, then it is necessarily to increase the tensile load again to set in motion dislocations fixed in a neighborhood adjacent to the previous one. That's why, during the reloading, the AE activity rapidly decreases because many less dislocations can move.

4.3. Localization treatment

Localization of the acoustic events along the gauge length of the specimen, Fig. 7, shows that the Lüders band propagation is followed with a good enough resolution, unlike the necking for example. As seen previously thanks to the IRT technique, strain localization occurs near both fillet radius at the end of the elasticity and then, a band with a high strain rate (= high density of events) propagates along the specimen.

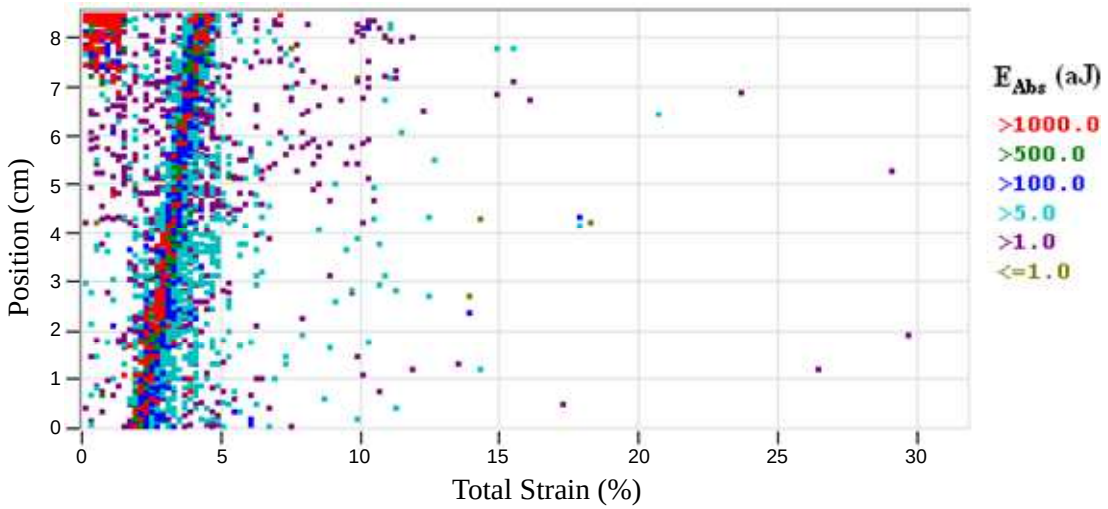

Figure 7. AE sources localization during tensile test on C35 steel.

Spatial distribution of the acoustic events is also correlated with their absolute energy. It can be observed that the most energetic events are localized at the band front. The reason is certainly due to a higher local dislocation activity, what is consistent with the dislocations avalanches which occur gradually at the band front. By keeping only events whose the absolute energy is higher than 500 aJ, a fortiori the most representative of the local strains, the standard deviation obtained on the Lüders band localization is less than 2 mm.

It can be noticed on Fig. 7, the band propagates at constant speed. This speed is about 40 times the crossbeam speed of the tensile machine. Others tests with a crossbeam speed varying between 0,02 and 1 $mm.min^{-1}$ on similar specimens led to the same result. Plekhov [28], in armco iron, finds also a linear dependence between the global deformation speed of the specimen and the propagation speed of the wave (Lüders band) where the plastic strains take place. In the SOLDUR 355 steel, Wattrisse [2] gets the same result.

4.4. AE – ESPI coupling results

To obtain good quality fringe patterns, crossbeam speed of the tensile machine was reduced to 0.02 $mm.min^{-1}$. All speckle patterns were saved manually, because of absence of automatic acquisition.

The Fig. 8 shows the very good correlation between both measurements techniques. As seen previously, at the beginning, plastic strains are localized in a fillet radius of the specimen (position between 0 and 1 cm). Then, when the stress is enough to activate gradually the slip systems in each grain of the gauge length of the specimen, deformation propagates at constant speed ($\approx 40 \times v_t$) by taking a localization band shape tilted of 58° with respect to the tensile axis.
It is interesting to note the inversion of the band inclination about half way (between fringe patterns 4 and 5 Fig. 8). This information can not be obtained with AE by using only two sensors. Thanks to the inclination angle measured on fringe patterns and the range of the AE zone along the specimen for a given total strain, it is possible to deduce the Lüders band width. This one is estimated to about 12 mm. Here, this value is not time dependent and about the same value was measured for different crossbeam speeds, in particular for the tests Fig. 7 (0.5 $mm.min^{-1}$) and Fig. 8 (0.02 $mm.min^{-1}$). Like for IRT, it is clear that Lorentz function applies on fringe patterns would give an integral band width depending on both the time elapsed to obtain these patterns and the crossbeam speed.
Fringes parallel to the tensile axis can be observed behind the band on several fringes patterns. These fringes, also parallel to the sensibility vector of the interferometer, show that the part of the specimen to the rear of the band rotates, as previously deduced by IRT. The same thing is more difficult to detect in front of the band, but these rotations can explain the AE activity outside of the band during its passing.

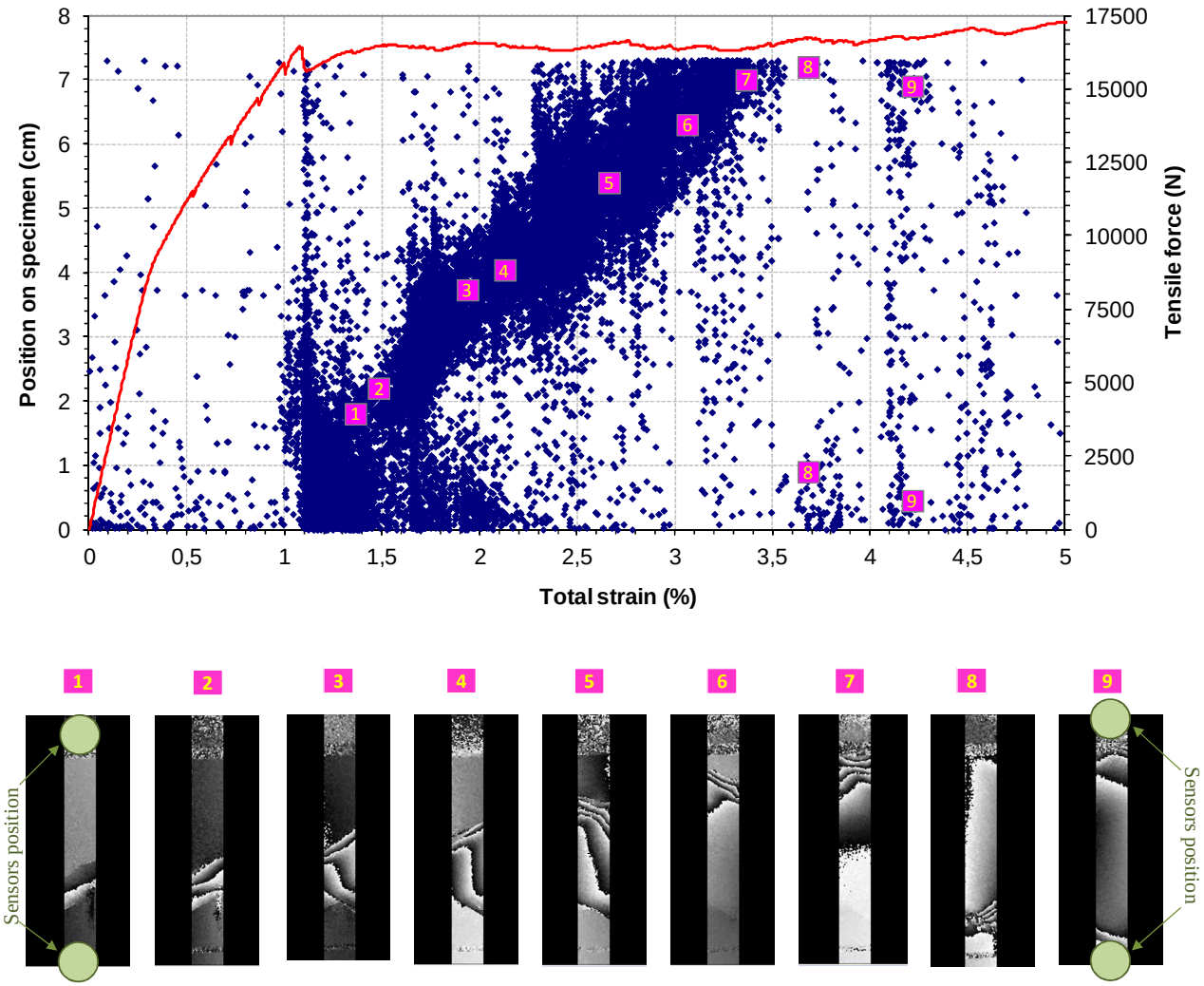

Figure 8. AE – ESPI coupling results collected while Lüders band propagation. The band position obtained by ESPI is reported on the AE data. A very good correlation is found between the two techniques.

Finally, by observing the evolution of the number of events on Fig. 6, one could think that the Lüders band propagates by jerks along the specimen, but according to ESPI results, the band propagation appears continuous. Indeed, it always exists a strain rate noticeably higher (presence of more close fringes) at the band front than in the rest of the specimen, on all fringe patterns, and it can be seen that the band front moves at constant speed from the ESPI pictures. However, jerky propagation of the band could not be measured if the break time or the slowing down of the band is less than the speckle patterns acquisition frequency.

5. Comparison and conclusion

The phenomenon of Lüders band propagation was investigated by three full-field measurements techniques: Infrared Thermography (IRT), Electronic Speckle Pattern Interferometry (ESPI) and Acoustic Emission (AE). Band features such as the ratio crossbeam speed / propagation velocity, inclination angle and band width were reported for a S235 steel by IRT and for a C35 steel by AE – ESPI coupling.

For the two materials, band propagation velocity is much higher than the crossbeam speed. Moreover, for the S235, the ratio crossbeam speed / propagation speed is more than the C35's one, what is consistent with a Lüders plateau greater in the case of the S235. In the two cases, it can be seen this ratio is approximately equal to the length of the plateau, *i.e.* data on S235 and C35 confirm the following equation given by Hähner [1]:

$$v_t = \varepsilon_p \times v_{BPL} \tag{4}$$

where v_t is the crossbeam speed, ε_p the plastic strain reached at the end of the Lüders plateau and v_{BPL} the Lüders band propagation velocity. This equation comes directly from an analysis of the propagation of the plastic front by assuming that the plastic strain is constant in the band and null outside, like shown in Fig. 9.

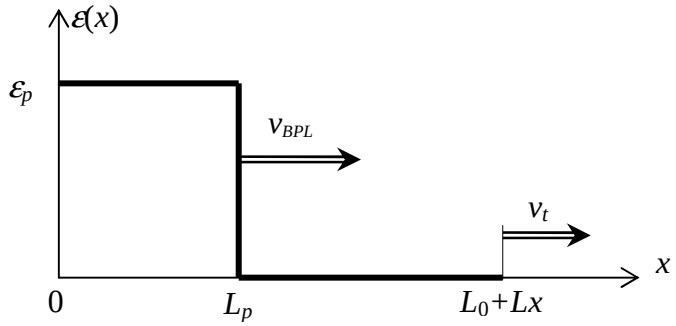

Figure 9. Scheme illustrating the propagation of the plastic front of a Lüders band.

So, the specimen elongation *Lx* would be only due to the propagation of the plastic front. AE measurements, Fig 7, confirm this hypothesis: there is only emission at the band front and, on each side of this front, there is a very weak acoustic activity, so no significant dislocation activity. When the length *Lp* travelled by the plastic front is equal to L_0+Lx (L_0: initial length of the specimen before the band apparition), the Lüders band crossed all the specimen and disappears.

The relation (4) was checked for the S235 at 10 mm.min^{-1} and for all experiments on C35 whatever the crossbeam speed between 0,02 mm.min^{-1} and 1 mm.min^{-1}, and it's found respectively : $\varepsilon_p = \frac{v_t}{v_{BPL}} \approx \frac{1}{24} = 4{,}1\%$ and $\varepsilon_p = \frac{v_t}{v_{BPL}} \approx \frac{1}{40} = 2{,}5\%$, what is close to the length of the experimental Lüders plateau on tensile curves (Fig. 2, Fig. 6 and Fig. 8). However, according to the temperature evolutions in front of the three points Fig. 2 and the relation Eq. 2, plastic strains inside the Lüders band could not be constant along the propagation and the modeling proposed in Fig. 9 would be unsuitable. More investigations have to be done.

For the two materials, the inclination angle with respect to the tensile axis is almost the same, 60° for the S235 and 58° for the C35. Nevertheless, this angle can vary and it was observed at the beginning of the test on the S235, the band was close to 90° and at half way of the band travel in the C35, the angle inverted, going from 58° to -58°.
Because of the movement of the band, it is difficult to measure a not time dependent band width. Yet, the AE – ESPI coupling allowed to introduce a way to determine a band width independently of the time and the crossbeam speed. But, accuracy of this method remains to define.
Concerning the band propagation, it was shown thanks to IRT, just behind the band, one part, the lower part for example, would be under purely elastic tensile stress while the other part, the upper part in this case, would be under purely elastic compressive stress. This particular mechanical state induces rotation of the part of the specimen located to the rear of the band. This assertion was confirmed by ESPI observations and, to a lesser extent, by AE.
Thanks to AE, important dislocations activity was observed during the Lüders band passing and correlation was found between the evolution of the dislocations activity and the tensile curve fluctuations. This serrated dislocations activity let think of a jerky propagation which seems in contradiction with ESPI and IRT (but on a different steel) measurements at the acquisition frequencies used. In fact, the bands determined by IRT and ESPI are obtained on time scales, relatively to the crossbeam speed, much smaller than the jerks measured by AE, what could explain the continuous aspect of the band get by IRT and ESPI, contrarily to the AE.
The following table, Table 2, summarizes the features of each technique and the measurements performed by.

Table 2. Technique features and possible Lüders band properties measurements.

Technique	**Type of propagation detected**	**Spatial resolution**	**Accuracy**	**Total strain rate (s^{-1})**	**Possibility of band inclination measurement**	**Possibility of band position estimation**	**Band velocity/ crossbeam speed ratio**
IRT	Continuous in S235 at 33Hz	0.25mm/pix	25mK on temperature	1.7×10^{-1}	Yes, 60° in S235	Yes	24
ESPI	Continuous in C35 at ~0.1Hz	5µm/pix	25nm on displacement 10^{-6} on strain	3×10^{-4} to 1.5×10^{-1}	Yes, 58°/-58° in C35	Yes	40
AE	Continuous but jerky at random time acquisition with a minimum interval of 2.10^{-5} s		±5mm on event localization		No with only 2 sensors	Yes	

At last, let's remind the two experiments were performed in two different laboratories, on two different tensile machines, with two different steels and at two different crossbeam speeds, what makes difficult the comparison between the techniques. Consequently, to refine this study, coupling of the three analysis techniques on the same material is being implemented.

References

[1] P. Hähner. Theory of solitary plastic waves – Part I: Lüders bands in polycrystals. *Applied Physics A Solids and Surfaces*, 1994, 58:41–48.

[2] B. Wattrisse, A. Chrysochoos, J.-M. Muracciole, M. Némoz-Gaillard : Kinematic manifestations of localisation phenomena in steels by digital image correlation. *Eur. J. Mech. A-Solids*, 20:189–211, 2001.
[3] O.A. Plekhov, O.B. Naimark, N. Saintier, T. Palin-Luc. Elastic–Plastic Transition in Iron: Structural and Thermodynamic Features. *Technical Physics*, 2009, 54(8):1141–1146.
[4] R. Shabadi, S. Kumar, H.J. Roven, E.S. Dwarakadasa. Characterisation of PLC and parameters using laser speckle technique. *MSEA*, 2004, 364:140–150.
[5] H. Neuhäuser, F.B. Klose, F. Hagemanna, J. Weidenmüller, H. Dierke, P. Hähner. On the PLC effect in strain-rate and stress-rate controlled tests–studies by laser scanning extensometry. *Journal of Alloys and Compounds*, 2004, 378:13–18.
[6] Q. Zhang, Z. Jiang, H. Jiang, Z. Chen, X. Wu. On the propagation and pulsation of Portevin-LeChatelier deformation bands: An experimental study with digital speckle pattern metrology. *Int. J. Plasticity*, 2005, 21:2150–2173.
[7] B. Guelorget, M. François, C. Vial-Edwards, G. Montay. Strain rate measurement by ESPI: A new look at the strain localization onset. *Mat. Science & Eng*., 2006, 415: 234–241.
[8] G. Montay, M. Francois, M. Tourneix, B. Guelorget, C. Vial-Edwards, I. Lira. Analysis of plastic strain localization by a combination of the speckle interferometry with the bulge test. *Opt. & Lasers Eng.*, 2007, 45:222–228.
[9] J. Petit, G. Montay, M. François. Localisation Phenomenon Investigation on SMATed Stainless Steel Samples by Speckle Interferometry. *Strain*, 2011, 47:363–371.
[10] P. Hogström, J.W. Ringsberg, E. Johnson. An experimental and numerical study of the effects of length scale and strain state on the necking and fracture behaviours in sheet metals. *International Journal of Impact Engineering*, 36 (2009) 1194–1203.
[11] F.B. Klose, F. Hagemann, P. Hähner, H. Neuhäuser. Investigation of the Portevin-Le Châtelier effect in Al-3wt.%Mg alloys by strain-rate and stress-rate controlled tensile tests. *MSEA*, 2004, 93:387–389.
[12] Z. Jiang, Q. Zhang, H. Jiang, Z. Chen, X. Wu. Spatial characteristics of the Portevin-Le Chatelier deformation bands in Al-4 at%Cu polycrystals. *MSEA*, 2005, 403:154–164.
[13] H. Dierke, F. Krawehl, S. Graff, S. Forest, J. Săchl, H. Neuhäuser. Portevin–LeChatelier effect in Al–Mg alloys: Influence of obstacles – experiments and modelling. *Computational Materials Science*, 2007, 39:106–112.
[14] N. Ranc, D. Wagner. Experimental study by pyrometry of Portevin–Le Châtelier plastic instabilities—Type A to type B transition. *MSEA*, 2008, 474(1–2):188–196.
[15] Z. Marciniak, K. Kuczyński. Limit strains in the processes of stretch-forming sheet metal. *Int. J. Mech. Sci.*, 1967, 9:609–620.
[16] R. Mahmudi. Plastic instability in equi-biaxial deformation of aluminium alloy sheet. *J. Mater. Process. Technol.*, 1996, 57:266–271.
[17] A.H. Cottrell. Report of the Bristol Conference on Strength Solids, *Phys. Soc. Lond.*, 1948, 30.
[18] W.G. Johnston and J.J. Gilman. *J. Appl. Phys*, 1959, 30:129.
[19] Louche, H., Chrysochoos, A. Thermal and dissipative effects of accompanying Lüders band propagation. *Materials Science and Engineering A*, 2001, 307(1-2):15-22.
[20] Chrysochoos, A., Louche, H. An infrared image processing to analyse the calorific effects accompanying strain localisation. *International Journal of Engineering Science*, 2000, 38:1759–1788.
[21] B. Guelorget, M. François, Guillaume Montay. Strain localization band width evolution by electronic speckle pattern interferometry strain rate measurement. *Scripta Materialia*, 2009, 60(8):647–650.
[22] R. Jones, C. Wykes. Holographic and Speckle Interferometry, 2nd edn. vol. 6, Cambridge Studies in Modern Optics, Cambridge University Press, Cambridge, 1989.
[23] G. Cloud. Optical Methods of Engineering Analysis, Cambridge University Press, NY, 1995.

[24] J. Roget. Essais non destructifs. L’émission acoustique. Mise en œuvre et application. AFNOR - CETIM, 1988.
[25] M. Grumbach, M. Prudhomme, Ph. Lemble. Lüders Bands Propagation At Steel Yield Point, Films. IRSID, 1962.
[26] P. Fleischmann, F. Lakestani, J.C. Baboux. Analyse Spectrale et Energétique d'une Source Ultrasonore en Mouvement – Application à l'Emission Acoustique de l'Aluminium soumis à Déformation Plastique. *Materials Science and Engineering*, 1977, 29:205–212.
[27] J. Baram, M. Rosen. Acoustic Emission Generated during the Tensile Testing of Aluminium Alloys. *Materials Science and Engineering*, 1979, 40: 21–29.
[28] O.A. Plekhov, O.B. Naimark, N. Saintier, T. Palin-Luc. Elastic–Plastic Transition in Iron: Structural and Thermodynamic Features. *Technical Physics*, 2009, 54(8):1141–1146.